SAND2015-9373

SANDIA REPORT

2015-0000
Unlimited Release
Printed October, 2015

Cohesive Zone Modeling in Geomaterial

Rachel Provost, Pania Newell, Edward Matteo

Prepared by
Sandia National Laboratories
Albuquerque, New Mexico 87185 and Livermore, California 94550

Sandia National Laboratories is a multi-program laboratory managed and operated by Sandia Corporation, a wholly owned subsidiary of Lockheed Martin Corporation, for the U.S. Department of Energy's National Nuclear Security Administration under contract DE-AC04-94AL85000.

Sandia National Laboratories

Issued by Sandia National Laboratories, operated for the United States Department of Energy by Sandia Corporation.

Available to DOE and DOE contractors from
U.S. Department of Energy
Office of Scientific and Technical Information
P.O. Box 62
Oak Ridge, TN 37831

Telephone: (865) 576-8401
Facsimile: (865) 576-5728
E-Mail: reports@adonis.osti.gov
Online ordering: http://www.osti.gov/bridge

Available to the public from
U.S. Department of Commerce
National Technical Information Service
5285 Port Royal Rd
Springfield, VA 22161

Telephone: (800) 553-6847
Facsimile: (703) 605-6900
E-Mail: orders@ntis.fedworld.gov
Online ordering: http://www.ntis.gov/help/ordermethods.asp?loc=7-4-0#online

2015-0000
Unlimited Release
Printed October, 2015

Cohesive Zone Modeling in Geomaterial

Rachel Provost
Master's Student,Civil Engineering
University of New Hampshire
Durham, New Hampshire 03824

Pania Newell
Computational Structural Mechanics and Application
Sandia National Laboratories
P.O. Box 5800
Albuquerque, New Mexico, 87185-MS 0840

Edward Matteo
Geoscience Engineering
Sandia National Laboratories
P.O. Box 5800
Albuquerque, New Mexico, 87185-MS0779

Abstract

The purpose of the two projects discussed in this report is to use the cohesive zone method to evaluate fracture properties of geomaterials. Two experimental tests, the push-out test

and the notched three-point bend test, were modeled computationally using finite element analysis and cohesive zone modeling to extract load and displacement information and ultimately determine failure behavior. These results are to be compared with experimental tests when they are available.

The first project used the push-out test to investigate the shear bond strength at the cement-shale interface. The second project explored the effects of scaling a notched three-point bending specimen to study fracture toughness characteristics. The bond strength and fracture toughness of a material and its interfaces are important parameters to consider in subsurface applications so that zonal isolation can be achieved.

Acknowledgment

Thank you to my two mentors Pania Newell and Ed Matteo. Their expertise was inspiring and their patience greatly appreciated. Without them, my experience at Sandia would not have been as successful and enjoyable as it was and I cannot express how thankful I am for all of their help and guidance.

Thank you to Elisa Borowski for answering any and all of my Abaqus and Cubit related questions and always willing to help.

Thank you to the team at the University of New Mexico including Dr. Taha, Ala Eddin Douba and Moneeb Genedy for keeping me updated on the experimental tests, answering my questions and providing helpful Abaqus tips.

Thank you to Steve Sobolik for taking the time to review my SAND report and provide suggestions.

Thank you to my manager, Kevin McMahon, for making it possible for me to be at Sandia this summer.

Thank you to my graduate advisor, Dr. Majid Ghayoomi, for encouraging me to apply for this internship and being a great resource throughout my academic career.

Contents

List of Figures

List of Tables

Chapter 1

Computational Modeling of Push-Out Test

Introduction

In the lifetime of a wellbore, there are many instances in which its integrity, or its ability to achieve zonal isolation, can be threatened by changes in temperature and pressure, chemical degradation, the construction of the wellbore and the state of the geomaterial before cement placement [12]. These changes induce a stress differential within the cement-steel and the cement-formation interfaces that influences their shear bond strengths [12]. Figure 1.1 shows a typical wellbore system which is made of a steel casing surrounded by a cement sheath and located in the subsurface compromised of varying geomaterial. If a fracture or microannulus is to occur within any of these regions (cement-steel or cement-formation), zonal isolation is violated, and the mobility of fluid is made possible. Figure 1.1, instance d. and e. shows fractures forming within the cement-formation interface, instance a. and f. shows a formation microannulus and instance b. shows a microannulus between steel and cement [11]. Most concerning is the potential for vertical movement of fluid through the subsurface, originating from a flaw or microannulus in one of these interfaces, which poses a threat to health and the environment [11].

One study that was done investigated the evolution of micro-annuli at the cement-steel interface by subjecting a wellbore model to various confining pressure and casing pressures to measure the response of the effective hydraulic aperture. For these experiments, it was found that confining pressure has a larger influence on the formation of hydraulic apertures than casing pressure [20]. Another study that was done compiled experimental data regarding compressibility and permeability at the cement-steel interface and historical data from a CO_2 injection site in Cranfield, Mississippi to produce a computational field model evaluating the stress present in the wellbore system [19]. Similarly, this project will use a combination of computational data and experimental data, as it is available, to evaluate the bond strength at the cement-formation interface.

There are not many studies that have been done with respect to the cement-formation interface. However, it is necessary to understand and consider the data obtained from the cement-steel studies because the state of this interface influences that of the cement-rock

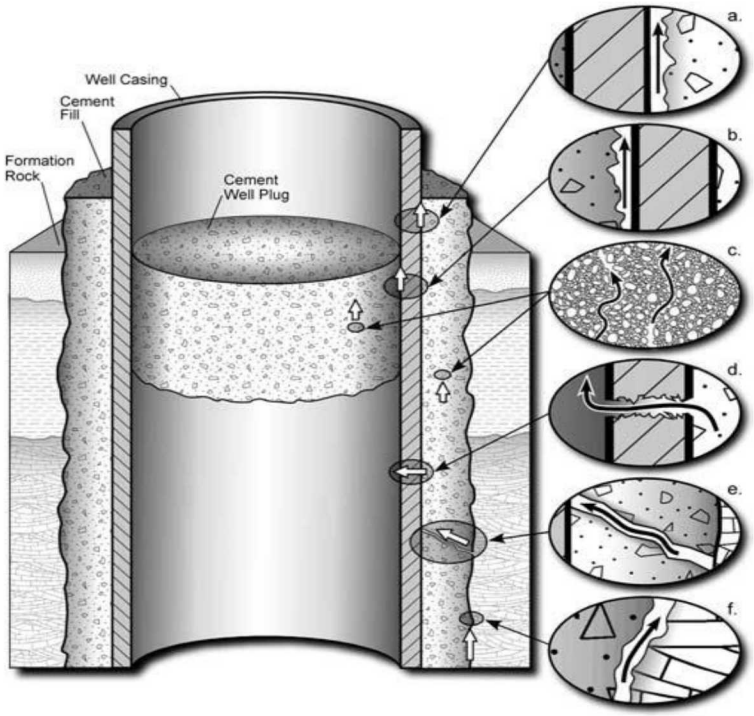

Figure 1.1. Schematic of a wellbore system demonstrating the various opportunities for microannulus or flaws to occur within the cement-steel and cement-rock interfaces [11]

interface [12]. The cement-formation interface, like the cement-steel interface, is vital in understanding and evaluating so that zonal isolation is accomplished and wellbore integrity is not diminished.

To investigate the bond strength between two different materials is a challenging task. Previous studies that have investigated the shear bond strength between two different materials concluded that the slant shear test was not an accurate experimental test to measure materials of varying stiffness. This was due to the tests inability to measure high areas of stress occurring along the interface [18]. The push-out test has been proposed to remedy this problem and accurately measure the shear bond strength at the cement- rock interface [12].

The push-out test is an appropriate test to measure the shear bond strength of the cement-shale interface because it can be subjected to a variety of temperature, pressure and chemical conditions. Shale has been chosen as the formation material because it has a significant presence in wellbore applications, accounting for up to 70 percent of the length of their footings. Depicted in Figure1.2 is a schematic of the push-out test to be used for the experimental portion of this project, which consists of a shale core surrounded by cement. A load will be applied to the shale core and the displacement of the shale will be measured by an LVDT.

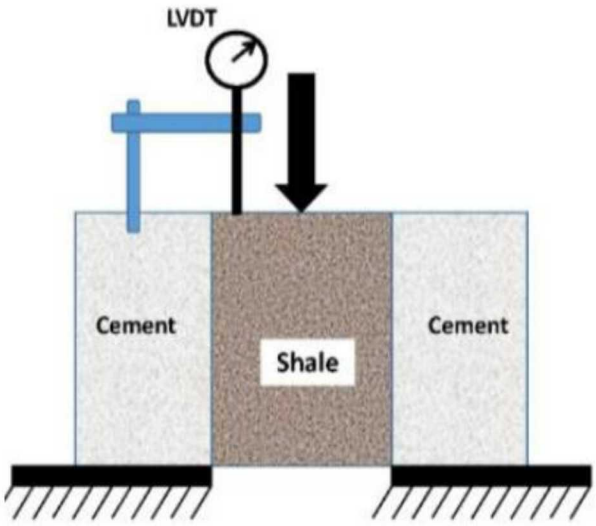

Figure 1.2. Schematic of push-out test to be used for experimental test [1]

This project will help determine whether or not the push-out test is an accurate method to measure bond strength between shale and cement by comparing the results from the experimental and computational tests. It will also provide more knowledge about the shear bond strength at the interface by exposing the system to different loading conditions to see how the interface reacts to environmental changes.

Methods

Learning ABAQUS

A cantilever beam example was used as an example to learn ABAQUS [2]. This was a valuable exercise in learning the different modules of the program and how to analyze the results. A distributed load of 500N was applied to a beam with dimensions and properties shown Figure 1.3, Table 1.1, respectively. The left end of the beam was fixed and the load was applied uniformly along the top surface of the beam as shown in Figure 1.4. The maximum principal stress contours of the beam are shown below in Figure1.5 for the refined model.

Table 1.1. Properties of material used for cantilever beam example

Property	Values	Units
Elastic Modulus, E	3.024E+6	Pa
Poisson's Ratio	0.26	-
Density	1893	kg/m^3

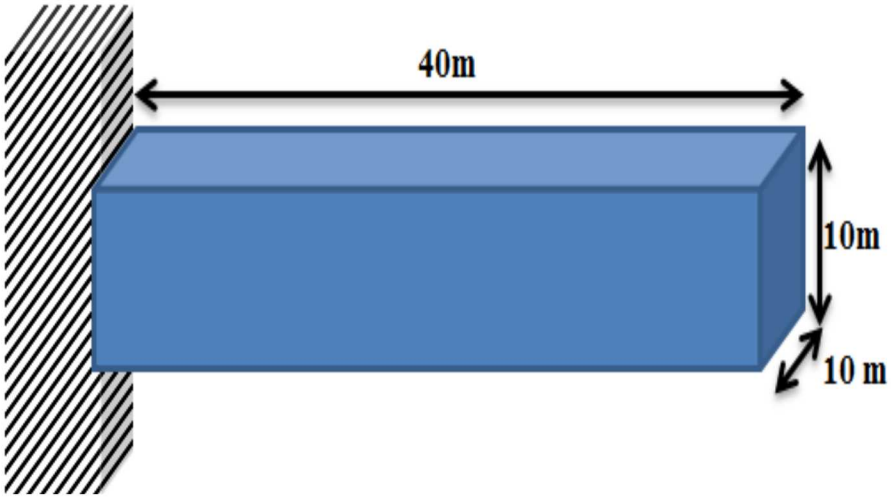

Figure 1.3. Dimensions and fixity of cantilever beam modeled in ABAQUS. Note: Figure 3 is not to scale

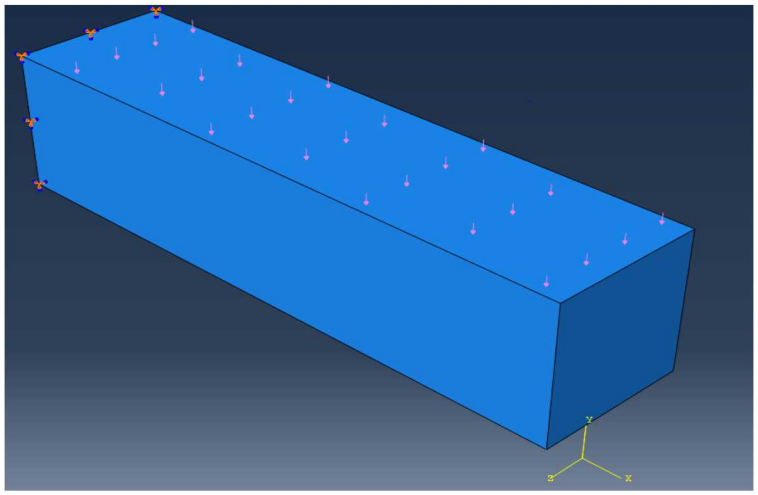

Figure 1.4. Cantilever beam with fixed end and distributed load as modeled in Abaqus

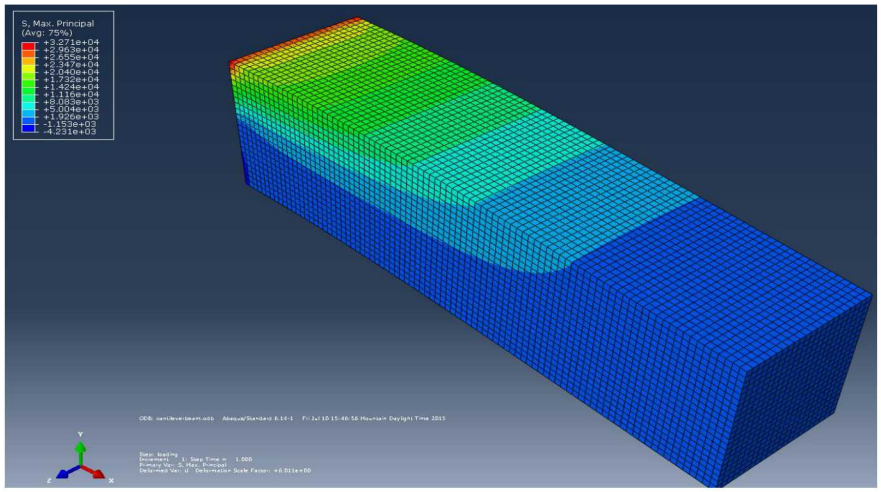

Figure 1.5. The maximum stress contours of the cantilever beam example

Different element sizes were used to make sure that the number of elements used for the analysis produced an accurate result. Shown in Table 1.2 are the tests that were done and their corresponding global seed sizes, number of elements and maximum stresses. The mesh was considered accurate for this example when there was little change in maximum stress based on the number of elements the model contained. Figure 1.6 shows the graph of number of elements vs. maximum stress. It should be noted that one needs to perform uniform mesh refinement analysis to investigate the convergence of this beam

Table 1.2. Global seed size, its number of elements, and the maximum stress

Global Seed Size	Number of Elements	Maximum Stress (Pa)
2	500	1.84 E+4
1.5	1323	2.04 E+4
1	4000	2.28 E+4
0.75	8957	2.48 E+4
0.6	19363	2.68 E+4
0.55	23652	2.74 E+4
0.5	32000	2.83 E+4
0.45	43076	2.92 E+4
0.4	62500	3.04 E+4

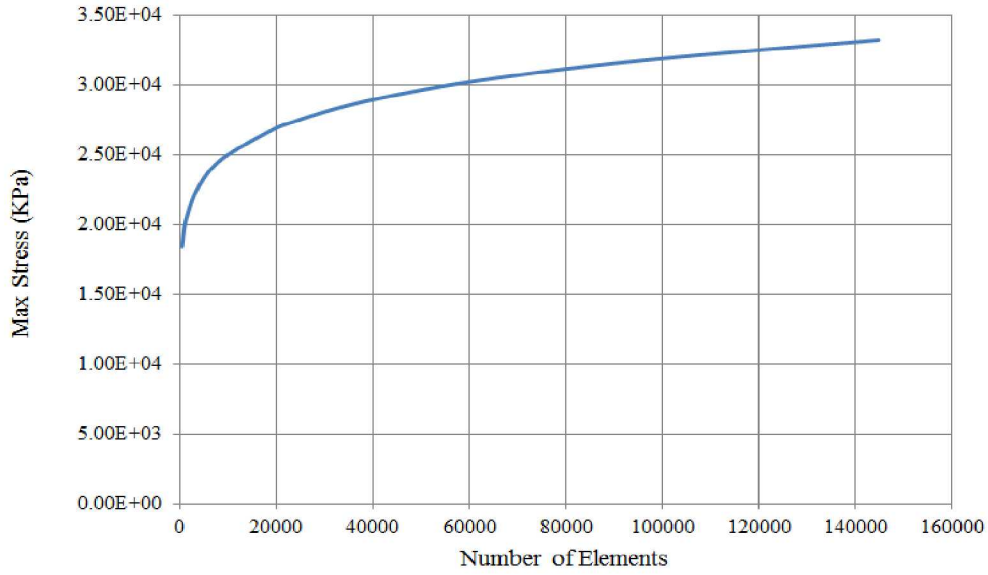

Figure 1.6. Graph of maximum stress vs. number of elements for the cantilever beam example

Cohesive Zone Modeling

The existing literature on fracture mechanics contains many methods of modeling processes in hopes of explaining the complexities of crack initiation and propagation while also pertaining to a variety of materials and environments. The cohesive zone method (CZM) was introduced by Barenblatt [17] to account for assumptions about the length and energy of the crack tip region and is often the preferred method of analyzing fracture processes due to its applicability to numerical approaches. The main similarities between the majority of these methods is their explanation of the traction-separation relationship. Figure 2.1 illustrates how both traction- the force at the interface, and separation- the distance between the interfaces, respond to a change in the other [17].

Shown below in Figure 2.1 is a traction separation curve that explains fracture initiation in terms of traction(τ)and separation of the material (). The stiffness of a material increases until it reaches its maximum traction(τ_0)at which point the traction then decreases until it equals zero and complete separation has occurred [15]. This bilinear approach is useful for brittle material such as concrete [21] [17]. Though this method assumes brittle behavior of the fractures it still provides a representation of the fundamental concepts of fracture processes. The area under this bilinear traction-separation curve is the fracture toughness, or G, a measure of the materials ability to resist separation calculated by the following equation 2.1.

$$G = 1/2 * \tau_0 * \delta_0 \tag{1.1}$$

The slope leading up to τ_0, or the traction at which maximum separation occurs, is the stiffness of the interface, or K. The separation traction is also the point at which maximum stress, σ_{max}, occurs. The following equation shows the relationship between these parameters [9].

$$K = \frac{\sigma_{max}}{\delta_0} \tag{1.2}$$

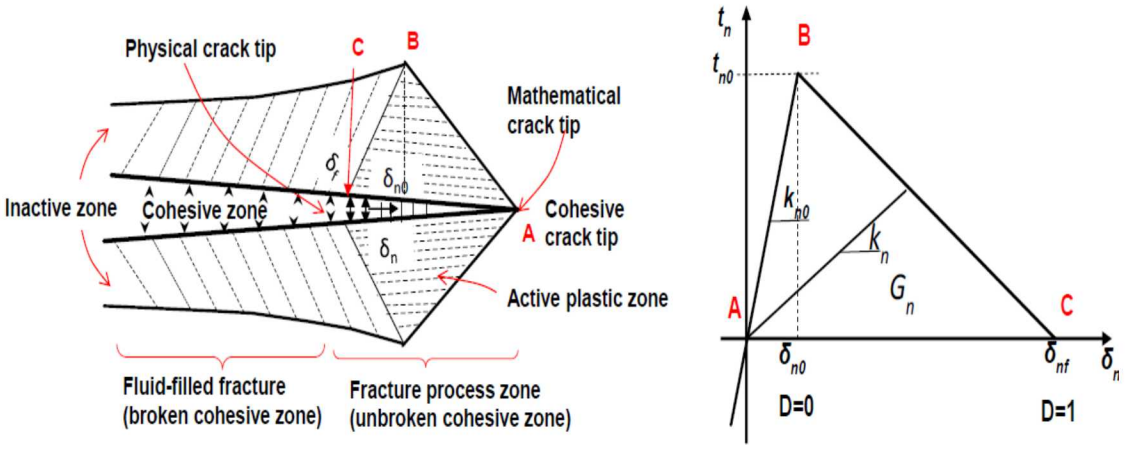

Figure 1.7. Traction-separation curve, shown on the right, and its corresponding locations within the fracture process zone, shown on the left [21]

For this project, cohesive zone modeling was used to understand the failure behavior of the cement-formation interface based on the law of traction separation. According to the cohesive zone method, the interface will fail, or separate, when a critical traction is applied. In the case of the cement-shale interface, the law of tractionseparation is a good method to use because it accounts for a wide variety of input parameters as is necessary in the case of two materials with different stiffness values [21].

Computational Modeling of the Push-Out Test

To obtain numerical information, ABAQUS [2] a commercial finite element analysis program, was used to model the push-out test. In ABAQUS, the cohesive zone of a model can be represented in a variety of ways. For the problem of the push-out test, the cohesive zone was modelled as its own separate part of zero thickness, with its own material properties, otherwise known as the cohesive crack method [21]. However, the cohesive zone can be modeled as a node-to-surface (or surface-to-surface) interaction in which its properties are defined within the interaction properties window [18].

The push-out test was modelled as shown in Figure 1.8. The model consists of five parts, two identical blocks representing the cement, one block with dimensions representing the shale, and two parts of zero thickness, representing the cement-rock interface. Dimensions of the setup are shown in Table 1.3 [21]. All of the parts were modeled as two dimensional planar shells.

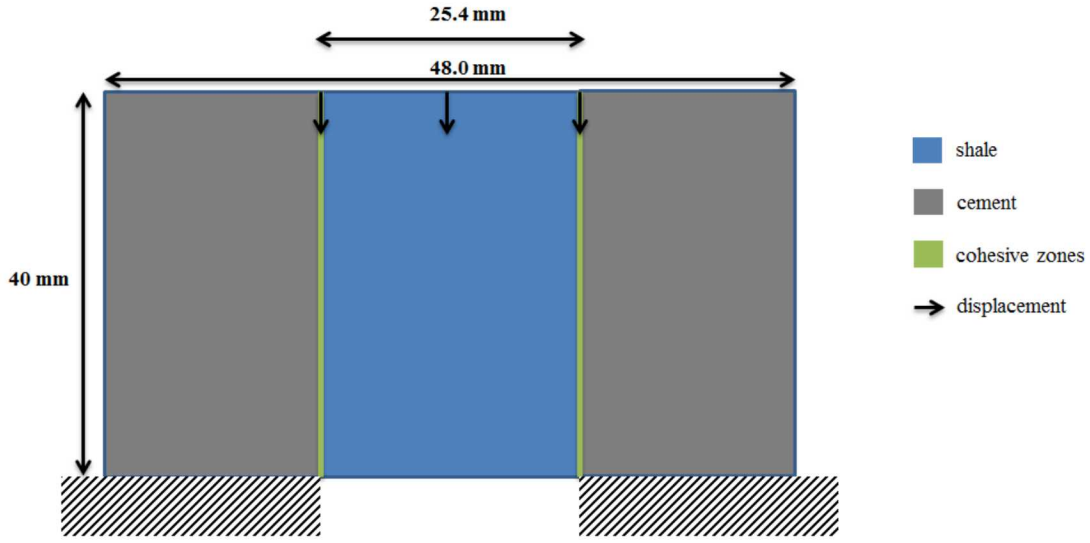

Figure 1.8. Abaqus model with boundary conditions and displacement

Table 1.3. Dimensions of the push-out test simulation in ABAQUS

Part	Dimensions(mm)
Cement	11.3x40
Shale	25.4x40
Cohesive	0x40

The cement ends were fixed according to the ENCASTRE type boundary condition, meaning that all displacements and rotations at these nodes were constrained, and placed in the automatically created initial step. A displacement was added to the top surface of the shale and characterized as a displacement/rotation boundary condition. This boundary condition was placed under the analysis step having a uniform distribution and a negative magnitude in the y-direction of 0.005 m/s.

Important values to consider when modeling the cohesive zone are the properties of the interface and bulk materials (cement and shale), and values that describe the damage initiation and evolution of the crack such as fracture energy and maximum traction [9]. In

the absence of experimental data, values from Wangs PhD. dissertation were used in this simulation as inputs for these values. However, if experimental data was available, these values could be determined by back calculating from the load displacement curve [18].

Each part was assigned a section with its respective material. The cement and shale sections were specified as solid, homogeneous sections with a linear elastic response and material properties seen in Table 1.4. The cohesive part was specified as a cohesive section with a traction separation response. The cohesive interface was assumed to have MAXPS (max principal stress) damage behavior, meaning the maximum principal stress was specified as well as a damage evolution relating to its fracture energy. The cohesive material was also assumed to follow the traction separation law as dictated by the inputs for the modulus of elasticity to shear modulus ratios. The input values for the cohesive zone material are shown in Table 1.5 [21].

Table 1.4. Input material properties of shale and cement

Property	**Part**	**Value**	**Units**
Modulus of Elasticity, E	Shale	3.25 E+6	KPa
	Cement	4.023 E+6	KPa
Poisson's Ratio,ν	Shale	0.26	-
	Cement	0.26	-
Density	Shale	2000	kg/m^3
	Cement	1893	kg/m^3

Table 1.5. Input material properties for the cohesive zone

Property	**Value**	**Units**
Maximum Principal Stress	420	KPa
Fracture Energy	100	$Joules/m^2$

There were four tie constraints, one for each edge of the cohesive zone, used in this model. Tie constraints were used so that the cement and shale parts could interact with the cohesive part even though they have different mesh sizes and element types. The master surface was defined as the non-cohesive part, either the cement or shale, and the slave surface was defined as the cohesive part. This was done because the cohesive zone will have a smaller mesh size than the cement and shale parts.

The interaction between the cement and shale allowed small sliding and its discretization method was surface to surface. The master surfaces were chosen as the cement parts and the slave surface was chosen as the shale part. Although it did not a make a difference in the results, this method was used for consistency. This interaction consisted of distinctive properties so its behavior could be accurately modeled as cohesive. These properties include determining the cohesive behavior of the interaction by allowing any slave nodes experiencing contact to be eligible slave nodes and specifying the stiffness coefficients as uncoupled with

a value of 3e6 KPa. The geometric properties of the interaction were also specified and the default out-of-place surface thickness or cross-sectional area was kept as the default value, 1.

A step was created for the analysis of the push-out test and described as static, general. This step also utilized the automatic stabilization and allowed damping factors from previous general step to be allowed in the analysis. The maximum ratio to strain energy used for this step was the default value of 0.05. The nonlinear geometry option was also turned on in the case that large deformations occurred. The loading or displacement conditions were placed in this step.

Each part of the model was meshed independent of the other parts. Single bias meshing was used in the cement parts of the model. This means that the mesh seeding became more frequent, or the element sizes became smaller, as the cement approached the interface. This was done by seeding the entire part and then seeding the top and bottom surfaces of the part on edge. The mesh was then applied to the cement. The shale was seeded according to double meshing. Like the cement, the top and bottom surfaces of the shale were seeded on edge however, instead of having only one end of decreasing mesh sizes, both edges had decreasing mesh sizes as they approached the interface for it is surrounded by cohesive zones on both sides.

A uniform mesh was used for the cohesive part. Also, because the cohesive part has zero thickness, the mesh size was smaller for this area than it was for the cement and shale parts. The cohesive was modeled as a cohesive mesh element. This was done because the interface has different properties, mentioned above that must be represented. Figure 1.9 demonstrates the single and bias mesh technique used for the cement and shale parts for the coarsest meshing case. The locations of the cohesive zones are in the areas of increased mesh density. Table 1.6 contains the number of elements and nodes of this model.

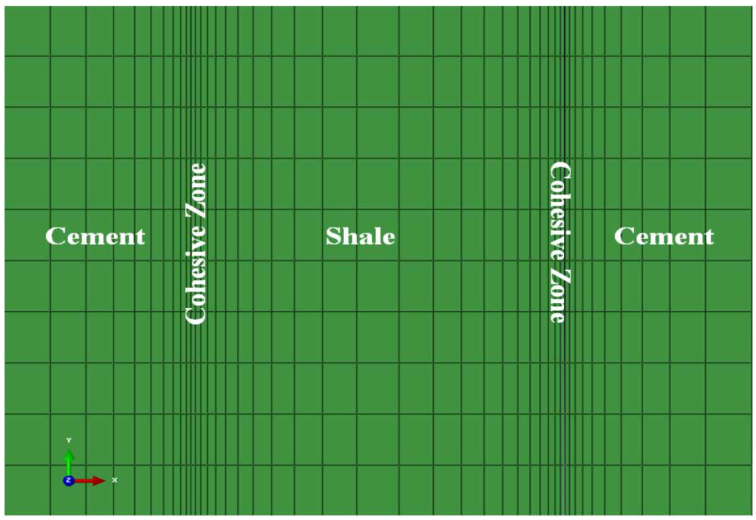

Figure 1.9. The meshing used to model the push-out test

Table 1.6. Number of element and nodes for each section of most refined case of the push-out simulation

Part	Number of Elements	Number of Nodes
Cement	220	253
Cohesive	133	268
Shale	440	495

Results and Discussions

A mesh sensitivity test was conducted to ensure that changing the mesh size would not affect the data output. Table 1.7 and 1.8 shows each part of the model and the number of elements that result from decreasing the seed size and therefore increasing the number of elements in each part. The number of elements is based on the global size of each seed. Figure 1.10 shows the graph of each refinement test and its force vs displacement curve. Case 1 represents the least refined model and Case 4 represents the most refined model. The difference between the peak loads of each model decreased meaning that the model is becoming more accurate and the refinement was stopped at Case 4 due to the limitations of the computing system. Figure 1.11 shows the stress contours of the maximum principal stress for the most refined case (Case 4).The location of this maximum value occurred at the node that was analyzed for further displacement and loading tests as well as the mesh refinement

Table 1.7. Each mesh refinement job and its corresponding max. and min. global seed size

Job Name	Part	Min. Global Seed Size	Max. Global Seed Size
Case 1	Cement	0.0003	0.003
	Cohesive	0.0003	0.0003
	Shale	0.0003	0.003
Case 2	Cement	0.0003	0.002
	Cohesive	0.0003	0.0003
	Shale	0.0003	0.0003
Case 3	Cement	0.00035	0.0015
	Cohesive	0.00035	0.00035
	Shale	0.00035	0.0015
Case 4	Cement	0.0003	0.001
	Cohesive	0.0003	0.0003
	Shale	0.0003	0.001

h

Table 1.8. Each mesh refinement job and its corresponding number of elements and nodes

Job Name	Part	Number of Elements	Number of Nodes
Case 1	Cement	90	110
	Cohesive	80	162
	Shale	190	220
Case 2	Cement	130	154
	Cohesive	100	202
	Shale	100	202
Case 3	Cement	160	187
	Cohesive	114	230
	Shale	320	363
Case 4	Cement	220	253
	Cohesive	133	268
	Shale	440	495

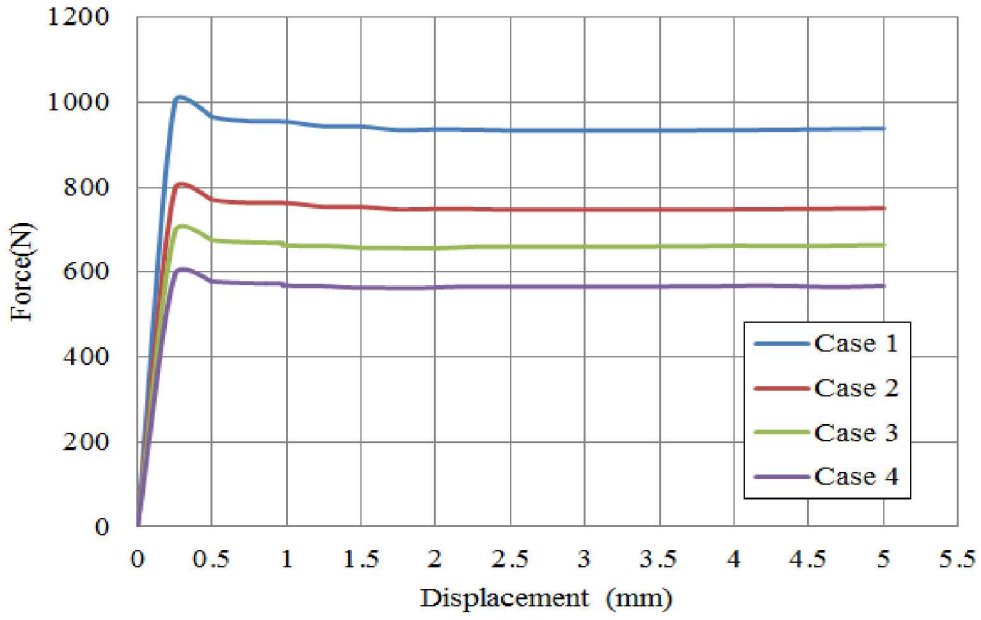

Figure 1.10. Mesh refinement analysis for a displacement of 0.005 m/s

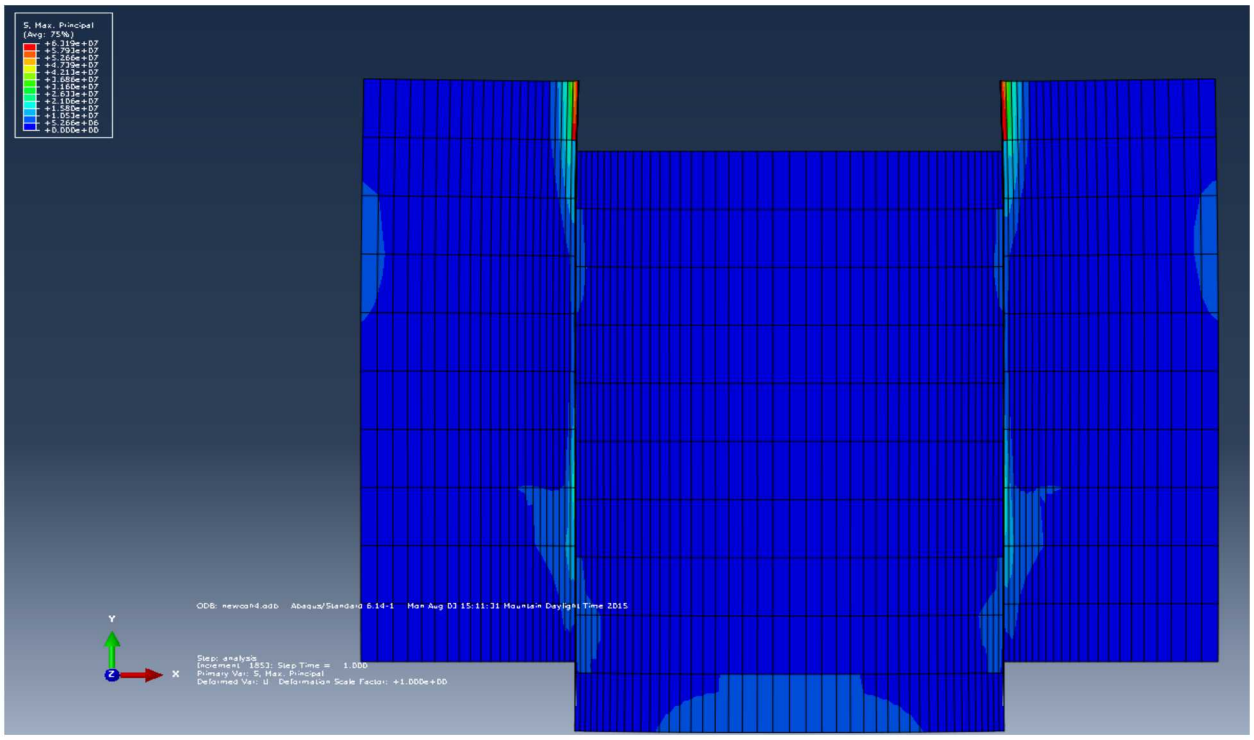

Figure 1.11. Maximum principal stress distribution for a displacement of 0.005 m/s.

The load vs displacement curve obtained from the literature is shown in Figure 1.12 and that obtained from this project is shown in Figure 1.12. The red box in Figure 1.12 from position 0 to 5 mm should be taken into consideration when comparing with the results from the computational test since that is the information available for this model as a result of 0.005 m/s displacement applied to the model. The fracture initiation behavior of the two plots are similar, as are their peak forces, however, it is unclear whether or not their softening behavior is similar.

Figure 1.13 suggests that the interfacial deformation is constant and that traction never reaches zero. However, this could change if a different displacement was applied to the model, or if the model was run longer, which is a topic requiring further investigation. The nonlinearity in the softening process (after the peak stress has been reached) could be a result of a mixture tensile and shear loading

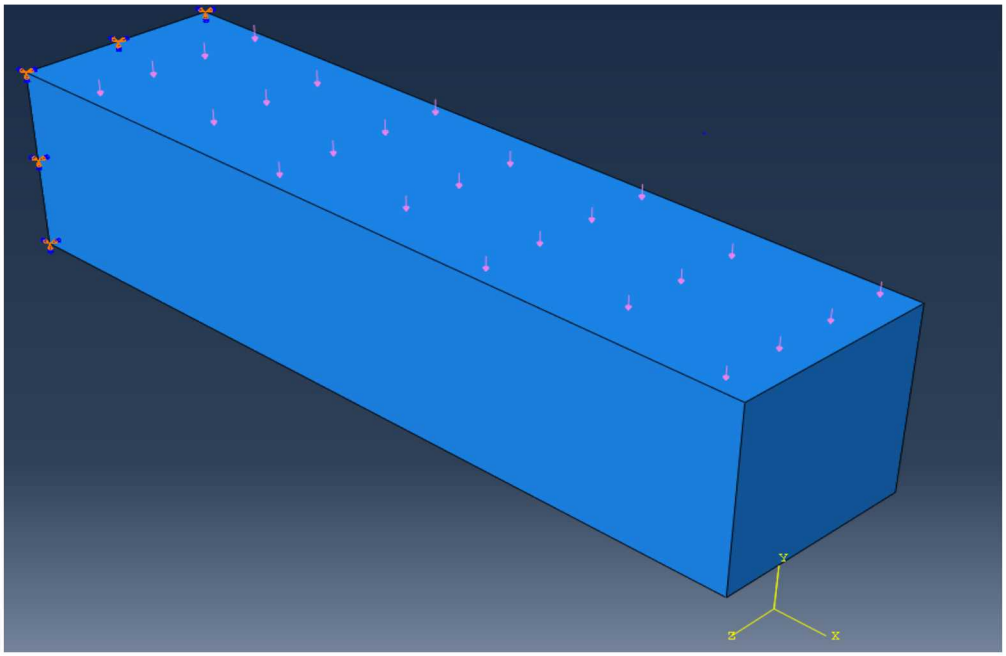

Figure 1.12. Force vs position graph for push-out test experiment [12]

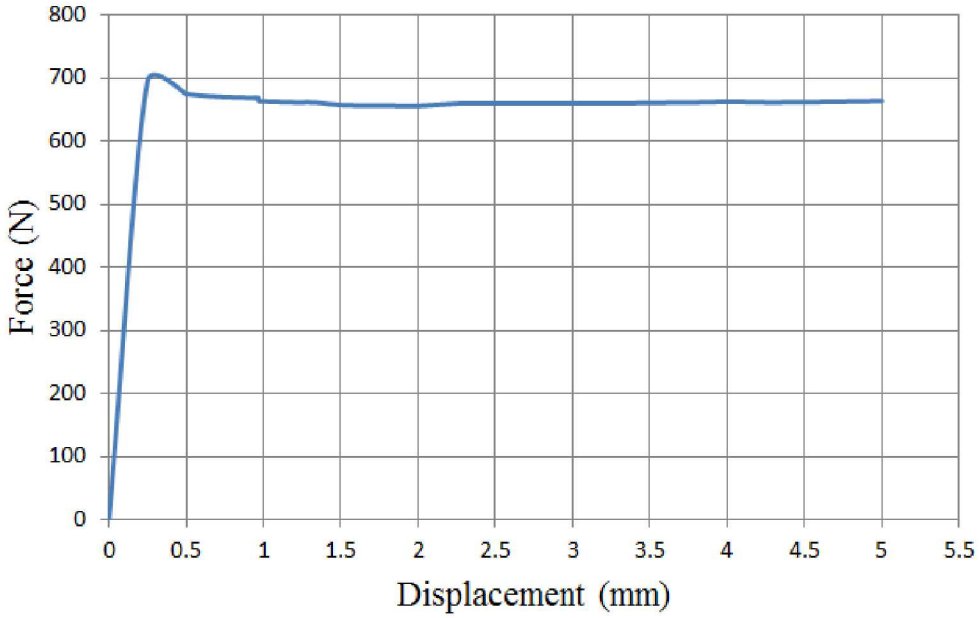

Figure 1.13. Force vs displacement results for one computational test of the push-out experiment.

Conclusion

The load/displacement behavior of the cohesive interface is similar to that described by the existing experimental data within the literature only in its initial linear trend up to its peak force, or up to the separation initiation. The softening of the interface is not similar to that explained by other scholars [12] [21]. Reasons for this may include that the push-out test does not account for any tensile force, which is a main contributor of fracture propagation and possibly interfacial deformation

Future Work

Of interest to this project is the injection of a repair material at the interface and its ability to reduce the likelihood of fracture initiation. This option has been investigated in the case of the steel-cement interface and it would be interesting to see how the repair material interacted with the cement-formation interface [13]. The shear bond strength is a good characteristic of the interface to compare between the samples with and without the repair material because shear force is the driving mechanism behind fracture initiation. It also may be of interest to explore the compressive strength of the interface since this is the property that dictates propagation of fractures [21].

Once more information about the experimental tests are available, this model can be used to simulate conditions that were tested in the lab to gather more information on the interfacial strength. Also, the load/displacement behavior at the cement-shale interface obtained from the computational tests along with experimental data, when available, can contribute to ongoing research about the necessary characteristics of the seal repair material and/or other solutions to achieve zonal isolation.

References

[1] Sandia and unm project description.

[2] Abaqus analysis user's guide, 2014.

[3] Cubit 15.0 user's manual, 2015.

[4] J. Planas, Z.P Bazant and M. Jirasek. Reinterpretation of karihaloos size effect analysis for notched quasibrittle structure. *International Journal of Fracture*, 111:17–28, 2001.

[5] Z.P. Bazant. Size effect. *Journal of Engineering Mechanics*, 110:518–535, 1984.

[6] Z.P. Bazant. Size effect. *International Journal of Solids and Structures*, 37:69–80, 2000.

[7] A.J. Rinehart, J.E. Bishop and T. Dewers. Fracture propagation in indiana limestone interpreted via linear softening cohesive fracture model. *Journal of Geophysical Research: Solid Earth*, 120(4):2292–2308, 2015.

[8] E. Borowski. Numerical investigation of fracture in geomaterial. Technical report, Sandia National Laboratories, 2015.

[9] A. Turon, C.G. Davila, P.P. Camanho and J. Costa. An engineering solution for mesh size effects in the simulation of delamination using cohesive zone models. *International Journal of Fracture*, 74:1665–1682, 2006.

[10] J. Ozbolt, R. Eligehausen and M. Petrangeli. Size effect in concrete structures. Technical report, Stuttgart University, Germany, 1994.

[11] S. Gasda and S. Bachu. Spatial characterization of the location of potentially leaky wells penetrating deep saline aquifer in a mature sedimentary basin. *Environmental Geology*, 46(6-7):707–720, 2004.

[12] H.J.K. Ladva, B. Craster, T.G.J. Jones, G. Goldsmith and D. Scott. The cement to fomration interface in zonal isolation. *SPE DrillingCompletion*, 20(3):186–197, 2005.

[13] S. Gomez. Wellbore microannulus characterization and seal repair: Computational and lab scale modelling. Master's thesis, University of New Mexico, 2015.

[14] B.L. Karihaloo. Size effect in shallow and deep notched quasi-brittle structures. *International Journal of Fracture*, 95:373–390, 1999.

[15] R. Kregtin. Cohesive zone modeling towards a robust implementation of more irreversible behavior. Technical report, Phillips Applied Technology, 2005.

[16] A. Hillerbourg, M. Modeer and P. Petersson. Analysis of crack formation and crack growth in concrete by means of fracture mechanics and finite elements. *Cement Concrete Research*, 6:773–782, 1976.

[17] C. Shet and N. Chandra. Analysis of energy balance when using cohesive zone models to simulate fracture processes. *Journal of Engineering Mechanics and Technology*, 124:440–450, 2002.

[18] A.E. Douba,E. Matteo,J. Stormont and M.M. Reda Taha. Apparent vs., true bond strength of steel and pc with nanoalumina. In *Proceedings of International Congress on Polymers in Concrete (ICPIC)*, pages 1–10, 2015.

[19] S.R. Sobolik, S.P. Gomez, E.N. Matteo, T.A. Dewers, P. Newell, J.C. Stormont and M. Reda Taha. Geomechanical modeling to predict wellbore stresses and strains for the design of wellbore seal repair materials for use at a co2 injection site. In *American Rock Mechanics Association. (ARMA)*, 2015.

[20] J.C. Stormont, R. Ahmad, J. Ellison, M.M. Reda Taha and E.N Matteo. Laboratory measurements of flow through wellbore cement-casing microannuli. In *American Rock Mechanics Association (ARMA)*, 2015.

[21] W. Wang. *Emergence of Delamination Fractures Around Casing and Its Stability.* PhD thesis, University of Wyoming, 2014.

Chapter 2

Scaling Effects of the Notched Three Point Bending Test

Introduction

Fracture mechanics is a field gaining lots of attention due to the many subsurface applications such as CO_2 sequestration, oil and gas production, and hydraulic fracturing presenting situations where fractures processes occur. These practices create a need for the phenomena of rock fracture to be understood and further investigated so that they can be carried out in a manner that is safe and effective. There are many methods whose goal is to explain fracture processes based on specific parameters and assumptions.

One of these methods, as explained in Chapter 1, but will be explained again here for the readers convenience, is the cohesive zone method (CZM). The existing literature on fracture mechanics contains many methods of modeling the cohesive zone method (CZM) in hopes of explaining the complexities of crack initiation and propagation while also pertaining to a variety of materials and environments. CZM was introduced by Barenblatt [17] to account for assumptions about the length and energy of the crack tip region and is often the preferred method of analyzing fracture processes due to its applicability to numerical approaches. The main similarities between the majority of these methods is their explanation of the traction-separation relationship, see Figure 2.1, and how both traction,, the force at the interface, and separation, the distance between the interfaces, respond to a change in the other [17].

Shown below in Figure 2.1 is the traction separation curve that explains fracture initiation in terms of traction (t) and separation of the material (). The stiffness of a material increases until it reaches its maximum traction (t_0) at which point the traction then decreases until it is equals zero and complete separation has occurred [15]. Figure 2.1 shows that the stiffness before and after separation is linear, suggesting that the stiffness does not change. This bilinear approach is useful for brittle material, such as concrete, when the original stiffness of the material is known [21] [17]. Though this method assumes brittle behavior of the fractures, it still provides a representation of the fundamental concepts of fracture processes. The area under this traction-separation curve is the fracture toughness, or G, a measure of

the materials ability to resist separation calculated by the following equation

$$G = 1/2 * \tau_0 * {}_0 \tag{2.1}$$

The slope leading up toτ_0, or the traction at which maximum separation occurs, is the stiffness of the interface, or K. The separation traction is also the point at which maximum stress,σ_{max}, occurs. The following equation shows the relationship between these parameters [15]:

$$K = \frac{\sigma_{max}}{\delta_0} \tag{2.2}$$

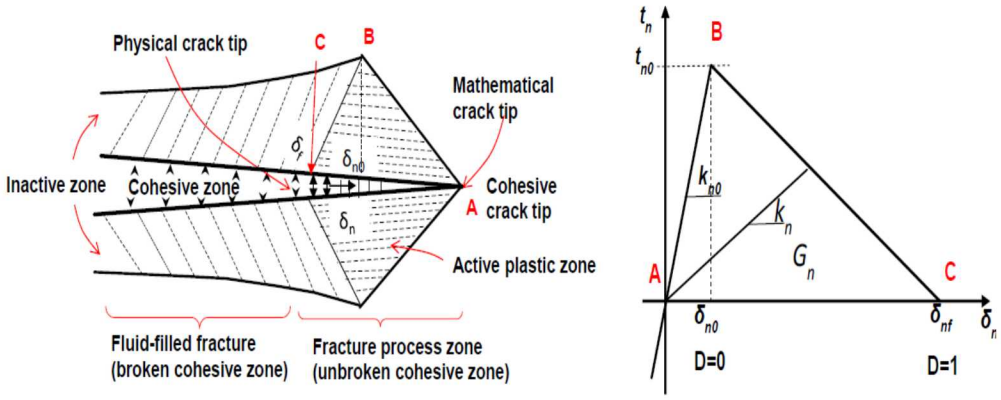

Figure 2.1. Traction-separation curve, shown on the right and its corresponding locations within the fracture process zone, shown on the left [21]

An approach to modeling fracture processes that uses CZM, linear softening cohesive fracture modeling (LCFM), involves certain assumptions to be made about the failure behavior of the material [7]. Both Rinehart et.al and Borowski focused on the influence of the geometry of a specimen in their studies, using linear softening cohesive fracture modeling (LCFM) techniques to explain fracture processes in the N3PB and short rod (SR) experimental tests of Indiana Limestone specimens. In order to understand fracture mechanics over a wide range of situations, it is important that the most thorough investigation of experimental results and assumptions made in modeling methods is conducted so that accurate prediction of fracture processes is possible [7] [8].

Rinehart concluded that the N3PB test is not accurately described by LCFM due to the assumption that failure mode is constant [7]. Borowski explained that this may be due to assignment of a single elastic moduli across the entire specimen when the assignment of

separate elastic moduli, one for tension and another for compression, reduces the disparity between computational data and experimental data [8]. This project will focus on the size effects of the N3PB to see how it influences fracturing behavior as it was cited by both Rinehart and Borowski as a topic that required more analysis in determining if LCFM is an appropriate method to model the N3PB experiment [7] [8].

Many studies [4] [16] [14] have explored the effects of scaling on the NP3PB test for concrete using various types of cohesive zone modeling procedures. Findings from these studies indicate that the softening curve, or the point at which traction decreases while separation continues to increase, changes based on the size of the N3PB concrete specimen [4]. This study critiqued a previous study [14] in which various assumptions about the size effects for the N3PB test lead to the formation of equations that produced illogical or incorrect values of important fracture process parameters such as fracture energy (G) and interface stiffness (K). A challenge posed in this study was the ability of a single equation to produce an accurate representation of these parameters for any specimen size or cohesive zone length [4] and is a topic of interest in this project.

Even though, there exist numerous studies that have investigated the size effect of the N3PB for concrete, very few of these studies have been applied to geomaterial. Incorrect assumptions that define the fracture as brittle, a result of the fracture process zone relative to that of the bulk material, may lead to incorrect analysis and may have significance in determining the most appropriate method of cohesive zone modeling for the N3PB experimental test. Also, another challenge when modeling fracture processes is limitations of sample preparation and acquisition of geomaterial, not present in concrete, and could benefit from the research done on sizing effects [7].

The N3PB, Figure 2.2, consists of a limestone section containing a notch, or a preexisting crack, in the middle of the specimen [4]. The cohesive zone, which represents the fracture process zone, is located in the middle of the specimen with a width smaller than that of the notch but whose length and depth extends throughout the entirety of the specimen. Figure 2.3 shows a cross sectional view of the notch and the cohesive zone within the specimen [7]. In this project, the N3PB simulation will be modeled computationally using the cohesive zone method, similar to that used in Chapter 1 for the push-out test using ABAQUS [2], which involves modeling the fracture process zone as a cohesive zone. A number of scaling cases will be conducted, changing both the limestone section and the cohesive zone width to see if and how size affects the load displacement curve and therefore fracture processes within the specimen.

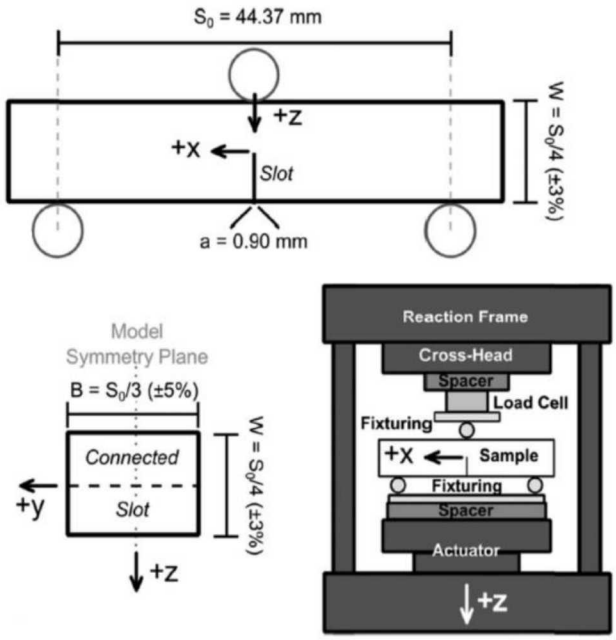

Figure 2.2. Schematic of the notched three point bending experimental test [7]

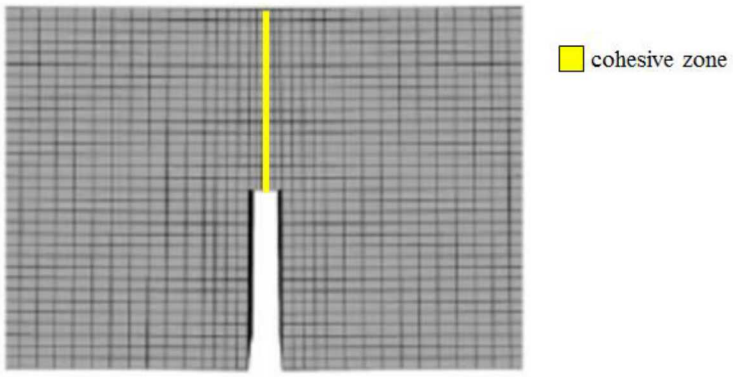

Figure 2.3. Cross-sectional view of specimen with notch and cohesive zone [7] modified by author

Methods

Base Case Reproduction and Scaling Cases

First, Rinehart et al.s computational test data was reproduced to ensure that the base case, or the case representing the specimens original non-scaled dimensions, could be used as an accurate reference to which the scaled cases could be compared. Figure 2.4 shows the reproduced base case to be the same as Rinehart et al.s so the reproduced case was selected as a base case for further analysis.

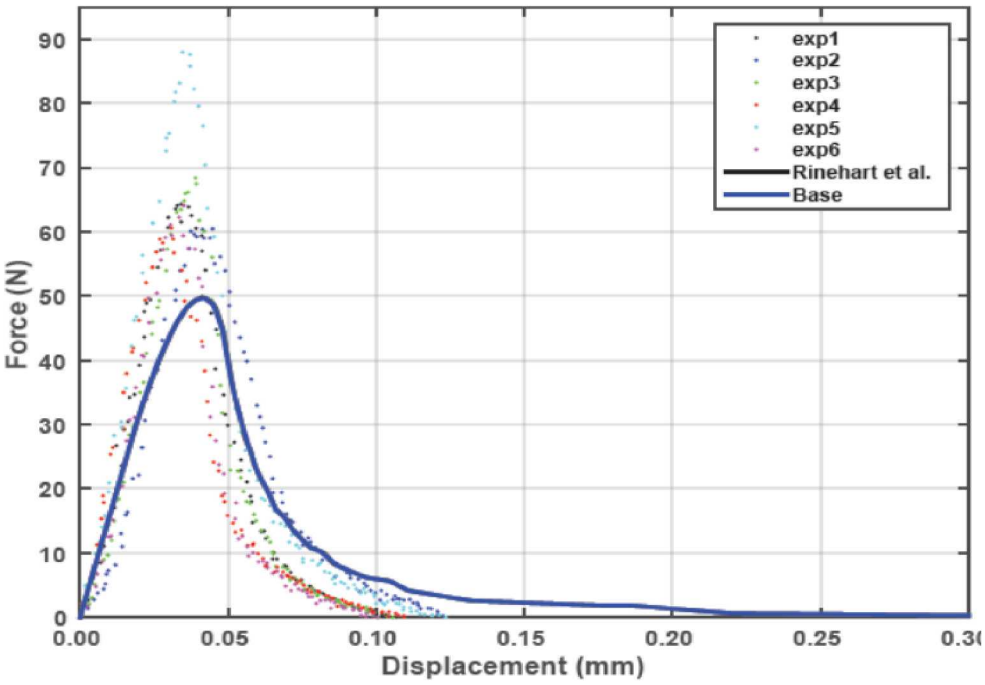

Figure 2.4. Force vs displacement base case verification

Once the base case was determined, the scaling factors could be applied to the specimen. There were two different types of scaling cases applied to the specimen for this study. The first set of cases involved scaling the entire beam but keeping the dimensions of the cohesive zone the same. The second set of cases scaled the width of the cohesive zone by first scaling the width of the notch but keeping the dimensions of the beam constant. Descriptions of each case, the part that was scaled, and the magnitude of the scaling is shown in Table 2.1 . The journal files, created in CUBIT, for each case can be found in Appendix B. Figure 2.5 and Figure 2.6 show the Case 0 (Base case) and Case 1 specimens and their dimensions as modeled in CUBIT [3].

Table 2.1. Each scaling case and its description

Case	Description
Case 0	Base Case
Case 1	Beam 2:1
Case 2	Beam 4:1
Case 3	Beam 1:2
Case 4	Beam 1:4
Case 5	Cohesive Zone 2:1
Case 6	Cohesive Zone 1:2

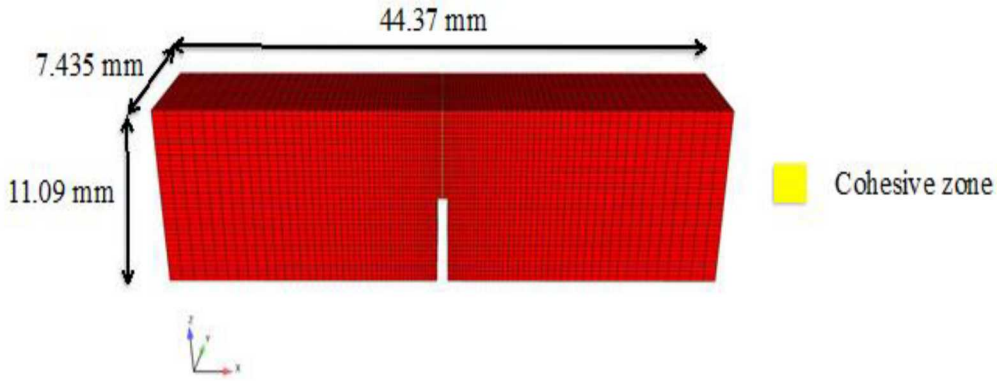

Figure 2.5. Base Case model

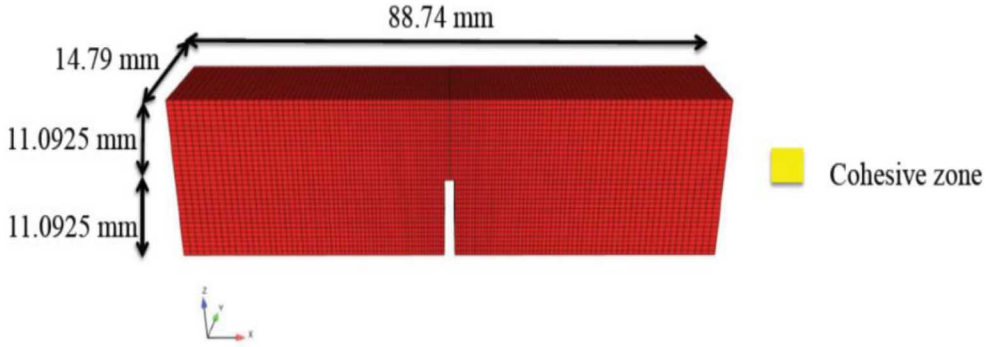

Figure 2.6. Case 1 model

Scaling the brick only required the length, width and height of the specimen to be multiplied by the appropriate scaling factor as indicated by its case. However, scaling of the

cohesive zone required more detail. Unlike the limestone specimen, changing of the cohesive zone changes the fracture behavior as explained by the cohesive zone method and its traction-separation curve. Changing the dimensions of the cohesive zone will change the shape of the traction-separation curve, however energy must be conserved and the area underneath the curve, or the fracture energy (G), must remain constant.

The original thickness of the cohesive zone was calibrated by Rinehart et al., in response to convergence difficulties arising from very small width in the cohesive zone. It was found that a cohesive zone width that was 10 percent of the width of the notch was the best option, resulting in a width of 0.09 mm used for the base case [7].

To change the width of the cohesive zone in a way that ensured fracture energy remained constant, the input file had to be changed accounting for the change in certain parameters. The fracture energy was found by integrating the load displacement curve resulting in a value of 0.0298 N/mm [7]. This value, along with the new length of the cohesive zone used in the following equation to find the new maximum traction, which is dependent on the cohesive zone length seen in equation 2.3.

$$l_{cz} = \frac{ME * G}{\tau_0^2} \tag{2.3}$$

Properties were determined through calibration process performed by Rinehart [7] and used in the test of the limestone (bulk material) and cohesive zone as shown in Table 2.2 and Table 2.3. The limestone was assumed to a have an elastic, isotropic behavior and the cohesive zone was modeled based on its damage evolution, or maximum stress and displacement possible at failure.

Table 2.2. Limestone Material Properties

Property	**Value**	**Unit**
Elastic Modulus,E	7	GPa
Poisson's Ratio,ν	0.28	-

Table 2.3. Cohesive Zone Material Properties

Property	**Value**	**Unit**
Elastic Modulus, E	38.9	GPa
Nominal Stress	5.9	GPa
Max. Displacement at Failure	0.0115	mm

Two different biases were used, extending in the x-direction, to cut down on computational cost and time while ensuring that the mesh of the cohesive zone was consistent to that

of its adjacent mesh in the rest of the specimen. Bias 1 was defined as the fine mesh and bias 2 was defined as the coarse mesh. Bias1 was determined based on a ratio corresponding to the original width of the notch (0.9mm). For each scaling case, the bias of the meshing had to be altered due to the change in size of the specimen or cohesive zone. Each case and its bias are shown in Table 2.4.

Table 2.4. Scaling cases and their corresponding bias meshing, number of elements and nodes

Case	Bias 1	Bias 2	Number of Elements	Number of Nodes
Base Case	0.9/4	Bias1*4.65	37856	42600
Case 1	0.9/4	Bias1*4.56	75488	84180
Case 2	0.9	Bias1*6.5	120288	133680
Case 3	0.9/4	Bias1*1.3	37856	42600
Case 4	0.9/8	Bias1*1.2	38304	43110
Case 5	0.9/4	Bias1*2.75	51296	57480
Case 6	0.9/15	Bias1*8.7	93408	104010

Results and Discussion

Figure 2.7 shows the effects of scaling on the limestone section of the beam. The experimental data is depicted by the dotted curves whereas the computational tests, labeled as Case 1, Case 2, Case 3, and Case 4, as well as the base case, are represented by a solid curve. It is evident that changing the specimen size has an effect on the N3PB test based on the difference in the peak force and corresponding displacement as compared to the base case.

Figure 2.7 indicates that with an increase in specimen size (Case 1 and Case 2) the peak force will also increase. The opposite is observed for Case 3 and Case 4; when the specimen size was decreased, there was a decrease in the peak force. The magnitude of the scaling also is significant. For Case 2, which involved scaling the specimen by a factor of 4, the peak force was around 500N whereas for Case 1, in which the specimen was scaled by a factor of 2, the peak force was around 160N. Case 2 results in a peak force almost four times larger than that of Case 1. Also, Case 1 results in a peak force more than double the peak force of the Base Case computational test. A 150N peak force for Case 1 was observed compared to 50N peak force for the Base Case.

Scaling the specimen by a factor to make it smaller produced a similar trend. The smaller the beam, the smaller the peak force observed. Case 3 shows a peak force of 25 N, which is about half of the peak force of the Base Case. Case 4 shows a peak force half of about 10N, which is around half of the peak force for Case 3. Based on Bazant's law of size effect, size effect occurs when there is a discrepancy in energy release rates between specimens [6]. There are two instances in which size effect can occur, one of them being from a statistical representation of the material such as location and magnitude of voids, cracks, etc. the other

is from the energy distribution within the material [6].

These results for Cases 1-4 are not consistent with the results produced by Bazant's work [5]. Bazant showed that with an increase in specimen length, there will be an increase in nominal strength whereas the opposite occurred in this analysis of Cases 1-4 [5]. This could be due to neglecting to address certain assumptions when investigating the law of size effect [10]. The assumptions that must be made include that: fracture energy, G,does not rely on the specimen size, the produced energy due to fracture propagation depends on the length and area of the fracture process zone,specimens must be geometrically similar and failure cannot occur in order to be considered for the size effect law to be applicable [10].

Also, in this analysis, the size effect of scaling the specimen only and not the cohesive zone could be due to a number of factors, conversely explained by Bazant's size effect law. Bazant's work is applicable for small beams rather than larger beams so it may be that the tests done for the beams of increasing size ie: Case 1 and Case 2, do not provide an accurate representation of specimen sizes that can be analyzed using this size effect law [6].

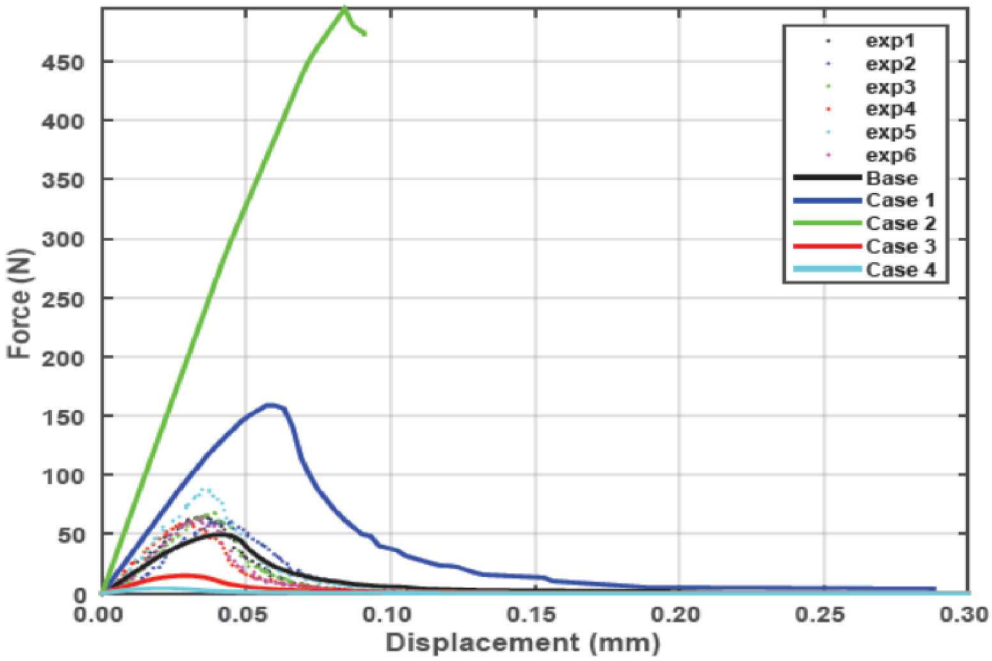

Figure 2.7. Force vs displacement curve for Cases 1, 2, 3 and 4

Figure 2.8 illustrates the effect that scaling the cohesive zone has the on the load displacement curve for the N3PB test. For Case 5, which contained a larger cohesive zone, the peak force was around 27N, about half of the original peak force obtained from the Base Case. However, for Case 6, which included a smaller cohesive zone, the load displacement curve was slightly changed and the peak force only decreased by a small amount to 48N.

This is different from Cases 1-4 which show a trend based on the magnitude of the scaling. See Figure 2.9 for the load displacement curve comparison for all of the cases. Also different between scaling the specimen versus scaling the cohesive zone is that the type of scaling factor (larger or smaller) produces opposite results.

As previously mentioned, the change in a specimen size of a geometrically similar specimen creates a difference in energy release rates, influencing the nominal stress of the specimen [6]. However, in Case 5 and Case 6, the specimen size did not change, the length of the cohesive zone did, and the nominal stress was still effected. This could be explained by the cohesive zone length equation seen in equation 2.3 which is dependent on the fracture energy and fracture energy. When the cohesive zone length increases, the fracture energy increases, requiring a larger nominal stress.

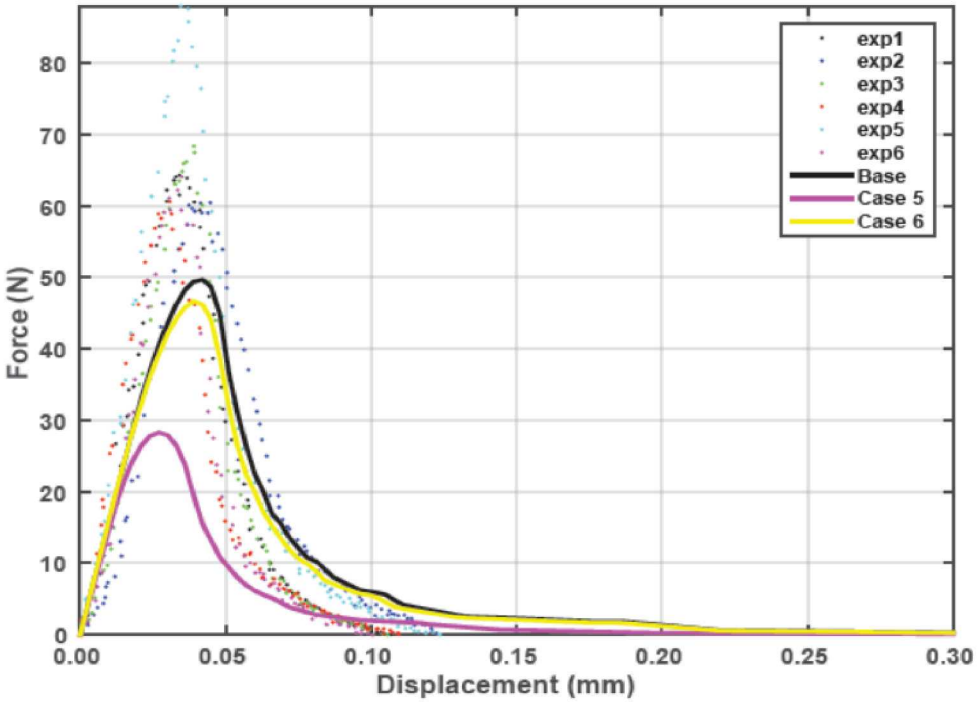

Figure 2.8. Force vs displacement curve for Case 5 and Case 6

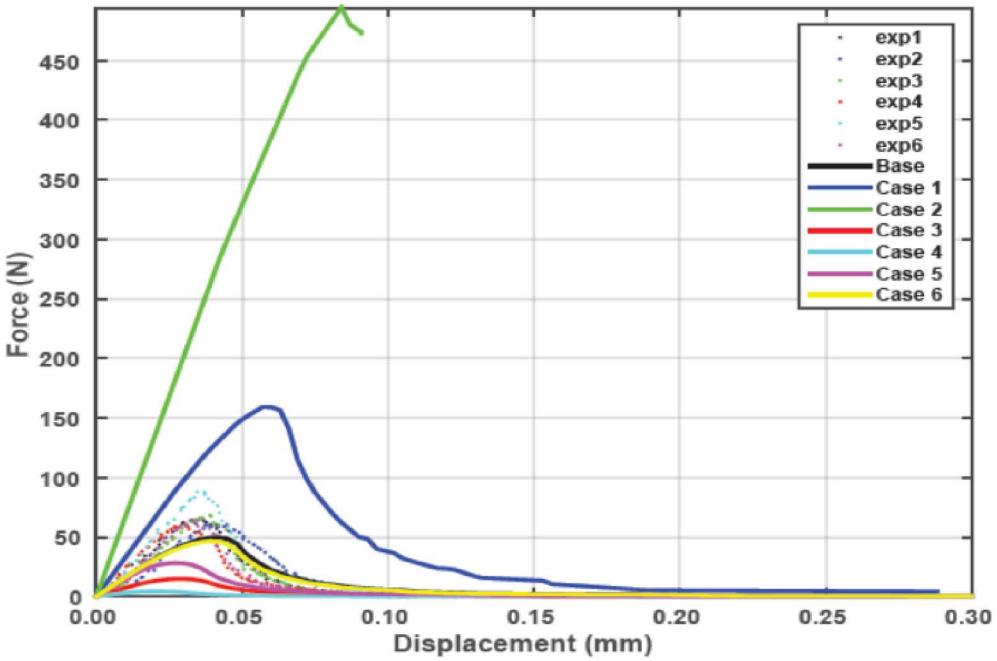

Figure 2.9. Force vs displacement curve for all cases

Conclusion

For the cases that scaled the limestone specimen and kept the cohesive zone the same, there was a consistent trend that suggests that with an increase in specimen size, the peak force will increase accordingly. These results not only indicate the trend of the sizing effect but its significance as well. In the case of scaling the cohesive zone and keeping the entire specimen the same size, there was a difference in its influence on the peak force; when increasing the size of the cohesive zone, the peak force decreased and vice versa for scaling the specimen. However, more tests need to be run to see if there is a trend between the magnitude of the scaling and the peak force. These results can be used to further analyze some of the assumptions made in LCFM about size of the specimen and cohesive zone, relative to the size of the fracture.

Future Work

Continuing this study would include investigating the scaling effects for the short rod test. This would hopefully indicate whether or not LCFM is a valid approach to cohesive

zone modeling in the event of different geometry and specimen sizes of experimental tests. A journal paper with Elisa Borowski will use findings from this paper to further investigate size effects of the notched three point bending and short rod experimental tests.

References

[1] Sandia and unm project description.

[2] Abaqus analysis user's guide, 2014.

[3] Cubit 15.0 user's manual, 2015.

[4] J. Planas, Z.P Bazant and M. Jirasek. Reinterpretation of karihaloos size effect analysis for notched quasibrittle structure. *International Journal of Fracture*, 111:17–28, 2001.

[5] Z.P. Bazant. Size effect. *Journal of Engineering Mechanics*, 110:518–535, 1984.

[6] Z.P. Bazant. Size effect. *International Journal of Solids and Structures*, 37:69–80, 2000.

[7] A.J. Rinehart, J.E. Bishop and T. Dewers. Fracture propagation in indiana limestone interpreted via linear softening cohesive fracture model. *Journal of Geophysical Research: Solid Earth*, 120(4):2292–2308, 2015.

[8] E. Borowski. Numerical investigation of fracture in geomaterial. Technical report, Sandia National Laboratories, 2015.

[9] A. Turon, C.G. Davila, P.P. Camanho and J. Costa. An engineering solution for mesh size effects in the simulation of delamination using cohesive zone models. *International Journal of Fracture*, 74:1665–1682, 2006.

[10] J. Ozbolt, R. Eligehausen and M. Petrangeli. Size effect in concrete structures. Technical report, Stuttgart University, Germany, 1994.

[11] S. Gasda and S. Bachu. Spatial characterization of the location of potentially leaky wells penetrating deep saline aquifer in a mature sedimentary basin. *Environmental Geology*, 46(6-7):707–720, 2004.

[12] H.J.K. Ladva, B. Craster, T.G.J. Jones, G. Goldsmith and D. Scott. The cement to fomration interface in zonal isolation. *SPE DrillingCompletion*, 20(3):186–197, 2005.

[13] S. Gomez. Wellbore microannulus characterization and seal repair: Computational and lab scale modelling. Master's thesis, University of New Mexico, 2015.

[14] B.L. Karihaloo. Size effect in shallow and deep notched quasi-brittle structures. *International Journal of Fracture*, 95:373–390, 1999.

[15] R. Kregtin. Cohesive zone modeling towards a robust implementation of more irreversible behavior. Technical report, Phillips Applied Technology, 2005.

[16] A. Hillerbourg, M. Modeer and P. Petersson. Analysis of crack formation and crack growth in concrete by means of fracture mechanics and finite elements. *Cement Concrete Research*, 6:773–782, 1976.

[17] C. Shet and N. Chandra. Analysis of energy balance when using cohesive zone models to simulate fracture processes. *Journal of Engineering Mechanics and Technology*, 124:440–450, 2002.

[18] A.E. Douba,E. Matteo,J. Stormont and M.M. Reda Taha. Apparent vs., true bond strength of steel and pc with nanoalumina. In *Proceedings of International Congress on Polymers in Concrete (ICPIC)*, pages 1–10, 2015.

[19] S.R. Sobolik, S.P. Gomez, E.N. Matteo, T.A. Dewers, P. Newell, J.C. Stormont and M. Reda Taha. Geomechanical modeling to predict wellbore stresses and strains for the design of wellbore seal repair materials for use at a co2 injection site. In *American Rock Mechanics Association. (ARMA)*, 2015.

[20] J.C. Stormont, R. Ahmad, J. Ellison, M.M. Reda Taha and E.N Matteo. Laboratory measurements of flow through wellbore cement-casing microannuli. In *American Rock Mechanics Association (ARMA)*, 2015.

[21] W. Wang. *Emergence of Delamination Fractures Around Casing and Its Stability.* PhD thesis, University of Wyoming, 2014.

DISTRIBUTION:

1	Dr. Majid Ghayoomi	
1	0751	Steve Sobolik, 6914
1	0779	Edward Matteo, 6222
1	0779	Kevin McMahon, 6222
1	0840	Pania Newell, 1555
1	0840	John Pott, 1555
1	0840	Jim Redmond, 1550
1	MS 0899	Technical Library, 9536 (electronic copy)


Sandia National Laboratories